View Article Online / Journal Homepage / Table of Contents for this issue

LAB ON A CHIP

Electrowetting-based actuation of droplets for integrated microfluidics†

M. G. Pollack,[a] A. D. Shenderov[b] and R. B. Fair*[a]

[a] *Department of Electrical Engineering, Duke University, Durham, North Carolina 27708, USA. E-mail: rfair@ee.duke.edu*
[b] *Nanolytics, Raleigh, North Carolina 27613, USA*

Received 15th November 2001, Accepted 21st February 2002
First published as an Advance Article on the web 11th March 2002

Published on 11 March 2002. Downloaded by Duke University on 10/04/2014 16:28:05.

The serviceability of microfluidics-based instrumentation including 'lab-on-a-chip' systems critically depends on control of fluid motion. We are reporting here an alternative approach to microfluidics based upon the micromanipulation of discrete droplets of aqueous electrolyte by electrowetting. Using a simple open structure, consisting of two sets of opposing planar electrodes fabricated on glass substrates, positional and formational control of microdroplets ranging in size from several nanoliters to several microliters has been demonstrated at voltages between 15–100 V. Since there are no permanent channels or structures between the plates, the system is highly flexible and reconfigurable. Droplet transport is rapid and efficient with average velocities exceeding 10 cm s^{-1} having been observed. The dependence of the velocity on voltage is roughly independent of the droplet size within certain limits, thus the smallest droplets studied (~ 3 nl) could be transported over 1000 times their length per second. Formation, mixing, and splitting of microdroplets was also demonstrated using the same microactuator structures. Thus, electrowetting provides a means to achieve high levels of functional integration and flexibility for microfluidic systems.

1 Introduction

In recent years, a major research effort has been directed towards the development of miniaturized chemical and biological instrumentation with a view to creating highly integrated and automated 'lab-on-a-chip' systems. Such systems offer many potential advantages, including reduced reagent consumption, smaller analysis volumes, faster analysis times, higher levels of throughput and automation, and increased instrument portability. Microfluidics has been the driving force behind the 'lab-on-a-chip' concept, but microliquid handling capabilities are still relatively primitive and inflexible compared to their macrofluidic (*e.g.* robotic) counterparts.

At present, most microfluidic technologies utilize closed channels permanently formed in glass, plastic or silicon through which continuous flows of liquid are pumped by either mechanical or electrokinetic means and where operations are carried out by changing the pressures or electrode voltages at strategic locations around the network.[1–6] Such systems suffer from drawbacks including complex fabrication, sample cross-contamination, high voltage or pressure requirements, large dead volumes, and complicated integration and control. Achieving high levels of functional integration is particularly challenging because fluid motion in any one part of the network typically depends on the voltages or pressures at multiple other locations within the network.

An alternative approach to traditional continuous-flow systems is systems based upon manipulation of discrete droplets. In such systems, unit-sized droplets of controlled volume and composition are dispensed from a source and subsequently transported through a network, with simple discrete operations such as mixing, reaction, incubation, splitting or sensing of droplets occurring at points along the way. In analogy to microelectronics we have sometimes referred to this approach as 'digital microfluidics'. Being conceptually similar to the manual operations in a bench-scale wet chemistry laboratory, digital microfluidics provides a way to directly transfer traditional protocols to microfluidic format. In contrast to continuous-flow microfluidics, little or no excess fluid is required to prime or fill microchannels so that much higher utilization of sample and reagent volumes is possible. A further significant advantage of droplet-based systems is that they are compatible with wall-less structures where the operations are carried out directly on the surface of a planar substrate, or between two substrates. Open structures are simpler to fabricate and assemble and, lacking fixed microchannels, they can be reconfigured more easily.

A number of techniques have been described for the actuation of microfluidic droplets including the use of air pressure,[7–9] thermocapillary effects,[10,11] electrochemical gradients,[12] structured surfaces,[13] photochemical effects,[14] dielectrophoresis[15] and other electrostatic techniques.[16–18] Many of these methods are based upon modulation of surface-tension, which is an attractive strategy for microdroplet actuation because of the favorable scaling of surface forces in the microdomain. Especially attractive are methods that modulate surface-tension at the solid–liquid rather than liquid–liquid interface as this permits greater control and localization of the force gradient. Through such localization microdroplets can be addressed and manipulated independently of one another leading to systems which are more flexible and scalable, and simpler to design and operate.

Electrostatic modulation of the interfacial tension between a solid electrode and conducting liquid phase is known as electrowetting.[19–33] Since electrical fields are easily modulated and can be precisely localized through the use of photolithographically defined electrodes, electrowetting can provide a very high level of control across the surface of a substrate. Electrowetting has previously been investigated for micro-

† Electronic supplementary information (ESI) available: six videos showing droplet flow, droplet dispensing and electrowetting. See http://www.rsc.org/suppdata/lc/b1/b110474h/

 DOI: 10.1039/b110474h

This journal is © The Royal Society of Chemistry 2002

View Article Online

Published on 11 March 2002. Downloaded by Duke University on 10/04/2014 16:28:05.

actuation in optical applications where the shape of a liquid lens was varied[29,30] or the capillary filling of a matrix of columns or porous material was controlled by an applied voltage.[19,20,31]

Colgate and Matsumoto[21] first proposed the use of electrowetting for micropumping of fluids in miniaturized closed-channel systems. An open-channel system in which droplets were electrostatically transported across a surface using an array of buried microelectrodes was first demonstrated by Washizu,[17] although it remains unclear whether this effect was due to electrowetting or an electrostatic body force.[34] We have previously demonstrated rapid electrowetting-based transport of droplets in air using a two-sided open-channel planar microactuator structure.[18] In the present work we extend these results to the transport of droplets in silicone oil media and present experimental results concerning the dynamics of droplet transport and the effect of scaling on transport rates. Additionally, we show that microdroplets can be split apart, merged together or dispensed from a fluid reservoir using the same microactuator structure. Thus, the key operations for a 'digital' microfluidic system are shown to be implemented in a single technology that is efficient, flexible, relatively simple to integrate and directly controlled by voltage.

2 Electrowetting microactuation

The electrowetting effect is illustrated in Fig. 1, where a polarizable and conductive liquid droplet is initially at rest on a hydrophobic surface. When an electrical potential is applied between the droplet and an insulated counter-electrode underneath the droplet, improved wetting is exhibited through a reduction in the droplet's contact angle with the surface. The improved wetting is a consequence of the lowering of the effective solid–liquid interfacial energy through electrostatic energy stored in the capacitor formed by the droplet–insulator–electrode system. The dependence of the effective soild–liquid interfacial tension, γ_{SL}, on the applied voltage, V, is given by Lippmann's equation:[22]

$$\gamma_{SL} = \gamma_{SL}^{0} - \frac{\varepsilon V^2}{2d} \quad (1)$$

where γ_{SL}^{0} is the interfacial tension at zero applied potential, and ε and d are the dielectric constant and thickness of the insulating film, respectively. The effect of the Debye layer in the liquid can be neglected since its capacitance is connected in series with the solid insulator, which typically has a much smaller capacitance. Consequently, the electrowetting effect is relatively independent of the concentration or type of ions in the solution.[28] Furthermore, the use of a solid insulator rather than a spontaneous space-charge layer to serve as the capacitor dielectric permits larger surface energies to be achieved at lower electric fields while greater control over the surface chemistry is possible. With proper selection of insulator materials relatively large and reversible contact angle changes have been demonstrated.[24,25,31,32]

Application of an electric field on only one side of the droplet creates an imbalance of interfacial tension which can drive bulk flow of the droplet.[35] This is the principle of the electrowetting-based microactuator shown in cross-section in Fig. 2. The droplet is sandwiched between two electrode planes and surrounded by silicone oil or other immiscible liquid or gas. The upper plate contains a single continuous ground electrode while the lower plate contains an array of independently addressable control electrodes each slightly smaller than the size of the droplet footprint. Both surfaces are hydrophobic and the control electrodes are electrically insulated from the liquid. The electrode size and droplet volume are designed such that when a droplet is centered upon an electrode it slightly overlaps all adjacent electrodes as well. In the work reported here we have used an interdigitated electrode shape to enhance the degree of overlap, although similar results have been obtained using simpler shapes such as squares or circles when the droplet is sufficiently large.

When all of the electrodes are grounded none of the capacitors formed by the droplet and each of the bottom electrodes is charged, and the energy of the system is independent of the position of the conductive droplet. If a sufficient voltage is now applied to an electrode on the bottom plate overlapping a portion of the droplet, the resulting surface energy gradient induces the droplet to move so as to align itself with the charged electrode. By successive electrode transfers droplets can be transported between any two addresses within the array. Since the control electrodes are insulated from the liquid both ohmic heating and undesired electrochemical reactions are prevented. With the same basic microactuator structure, different patterns of voltage activation or electrode arrangement can accomplish other manipulations, such as splitting, merging or dispensing of microdroplets from a larger source droplet.

Several possible microactuator electrode arrangements are illustrated in Fig. 3. The ground electrode may be either electrically insulated from [Fig. 3(a)] or directly in contact with the droplet [Fig. 3(b)]. When insulation is present on the ground electrode it should have a larger capacitance per area compared to the control electrode insulation so as to maximize the amount of electrostatic energy developed at the lower (*i.e.* asymmetrical) interface. If the capacitance between the droplet and ground electrode is too low, a position of minimum energy for the droplet may exist between the adjacent electrode centers, reducing the quality of alignment and making continuous transport difficult or impossible. In the limiting case where the ground electrode is absent (*i.e.* zero capacitance) [Fig. 3(c)] the droplet is expected to become 'stuck' midway between the electrode centers. At this position the potential differences between each of the control electrodes and the droplet have roughly the same magnitude but opposite polarity due to the

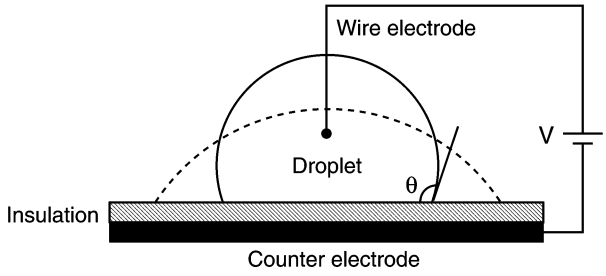

Fig. 1 The electrowetting effect. A droplet of conducting liquid initially forms a contact angle θ with a solid hydrophobic insulator (solid contour). Application of a voltage V between the droplet and a counter-electrode underneath the insulator reduces the solid–liquid interfacial energy, leading to a reduction in θ and improved wetting of the solid by the droplet (dashed contour).

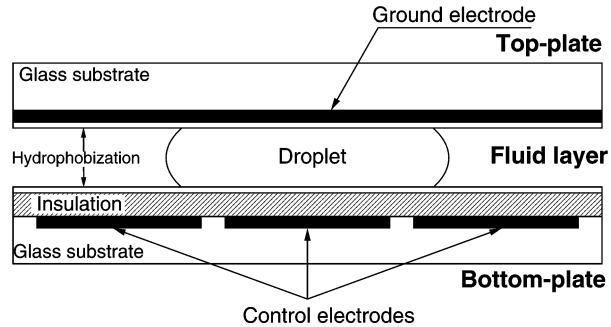

Fig. 2 Schematic cross-section of the electrowetting chip.

View Article Online

Published on 11 March 2002. Downloaded by Duke University on 10/04/2014 16:28:05.

geometrical symmetry. Since electrowetting is polarity-independent (eqn. 1) no surface energy gradient exists once the droplet reaches the midway point and this design is, therefore, expected to be unworkable.

On the other hand, droplets can be transported without an upper ground electrode if the control electrode pitch is sufficiently small compared to the droplet size, as shown in Fig. 3(d), which is essentially the design of Washizu.[17] However, this design requires a higher density of electrodes and is less amenable to two-dimensional array format. Alternatively, the ground plane may be coplanar with the control electrodes as a continuous network located in the spaces between or within the control electrodes if sufficient overlap of the droplet with both ground contacts and adjacent control electrodes can be maintained at all times [Fig. 3(e)]. Finally, both top and bottom plates may contain addressable control electrodes, as shown in Fig. 3(f). In this case, facing pairs of control electrodes can be simultaneously activated with voltages of opposite polarity to avoid the symmetry condition discussed in Fig. 3(c). While this design is probably the most difficult to fabricate and control, it is expected to be the most efficient due to the larger controllable interfacial area between the droplet and solid substrate.

In the experimental work reported here we have used a design which is electrically equivalent to Fig. 3(b). An 800-nm-thick film of parylene C provided insulation over the control electrodes and both top and bottom plates had a 60-nm-thick top-coating of Teflon AF 1600. The Teflon AF film provided a hydrophobic surface with a contact angle of 104° with water but was of insufficient quality to electrically insulate the ground electrode from the droplet. The control electrodes were patterned in a 200-nm-thick layer of chrome on a glass substrate using standard microfabrication techniques and the top-plate consisted of a glass substrate coated with a conducting layer (R_S < 20 Ω/square) of optically transparent indium tin oxide (ITO) to form the ground electrode. The gap spacing between the two plates was established by clamping the plates together with a glass spacer of known thickness. Prior to clamping the plates together, an electrolyte droplet of known volume was introduced with a pipettor. In some cases, smaller experimental droplets were dispensed from the initial source droplet using electrowetting forces, as described in Section 4. In all of the experiments reported here, the droplets were 0.1 M KCl solution, although we have observed no dependence on the salt concentration over the range 1–10^{-6} M. Electrical connection to the chip was made using a customized test-clip with spring-loaded pins and a computer-controlled custom-built electronic interface was used to switch the outputs. The output voltages were limited to 100 V dc and the polarity was positive with respect to the top-plate ground electrode, although no polarity dependence was observed in our experiments. The droplet transfer process is shown in Fig. 4 for a 900 nl droplet of 0.1 M KCl solution with electrode pitch L = 1.5 mm, gap spacing h = 0.3 mm and droplet diameter D = 1.9 mm.

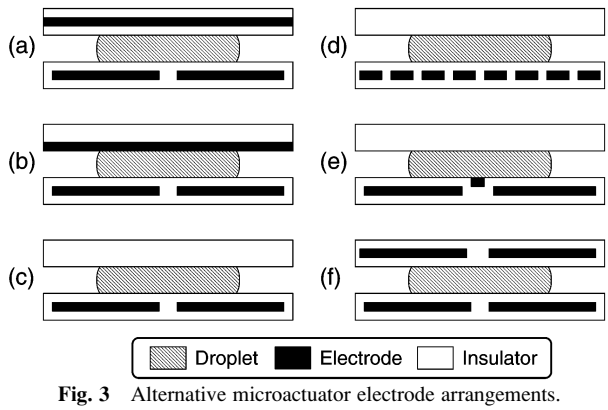

Fig. 3 Alternative microactuator electrode arrangements.

3 Droplet transport dynamics

Experiments were conducted to determine the voltage dependence and effect of certain parameters on droplet transport. The voltage-dependent maximum rate at which droplets could be transferred between adjacent electrodes was determined by oscillating a dc voltage pulse across a series of four adjacent electrodes at a fixed switching rate, f_s, while adjusting the voltage magnitude to find the minimum value at which a droplet could reliably follow the traveling pulse. At this voltage the time for the droplet to traverse an electrode, t_{tr}, is approximately equal to the switching period f_s^{-1}, and a voltage-dependent maximum rate of transfer is obtained. The average velocity of the droplet when switched at the maximum frequency is thus approximately $\bar{v} = Lt_{tr}^{-1}$, where L is the electrode pitch. Although $\bar{v}$ is the average velocity of a continually moving droplet, the instantaneous velocity is non-uniform as determined by video analysis of a droplet over the course of a single transfer (Fig. 5). Measurements using the voltage-balancing

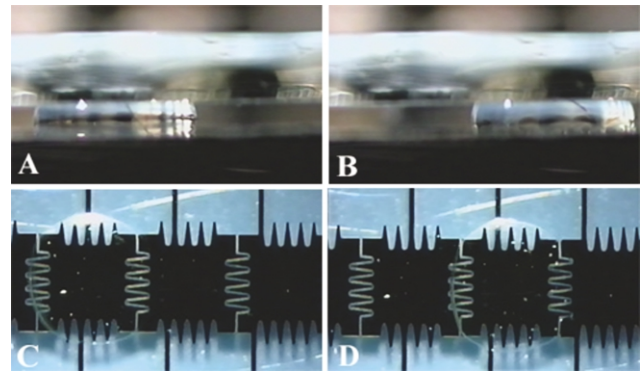

Fig. 4 Time-lapse series, droplet transfer. Moving droplets are imaged from the side (a), (b) and top (c), (d) at 66 ms intervals. The side-view droplet is in air, while the top-view droplet, seen through the transparent indium tin oxide ground electrode is bathed in silicone oil.

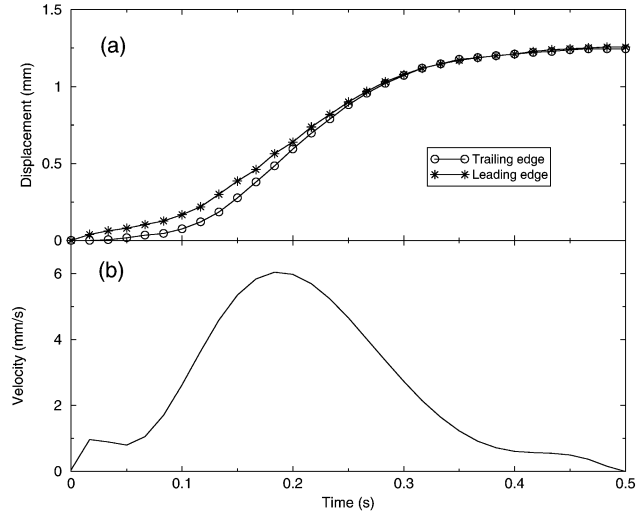

Fig. 5 Position and velocity of a droplet as a function of time during a single transfer determined by image analysis. (a) Displacement of the leading and trailing edges of the droplet with respect to their initial positions. Elongation of the droplet along the axis of motion is evident. The total displacement is less than the electrode pitch because of incomplete alignment due to the relatively low voltage used here. (b) Velocity of the droplet center determined by differentiation of a polynomial fit to the position data. The droplet was ~925 nl of 0.1 M KCl in silicone oil with L = 1.5 mm and h = 0.3 mm. The positional resolution of the image was 6 μm.

View Article Online

Published on 11 March 2002. Downloaded by Duke University on 10/04/2014 16:28:05.

technique compared well with rates determined by image analysis over the range where both methods could be applied.

Typical voltage characteristics for a 900 nl droplet of 0.1 M KCl solution with $h = 0.3$ mm and $L = 1.5$ mm are shown in Fig. 6 for both air and low viscosity (1 cSt) silicone oil media. In either medium a threshold voltage must be exceeded before any motion of the droplet is observed with this threshold voltage being much lower in oil than in air. It is well-known that equilibrium contact angles are typically not unique, but are characterized by a range a values with a lower limit, θ_R, for a contact line receding across a surface, and an upper limit, θ_A, for a contact line advancing across a surface.[36] Because of this contact angle hysteresis a threshold exists below which a contact angle imbalance does not result in motion of the contact line. We believe that contact angle hysteresis is responsible for the voltage threshold effect that we have observed for droplet transfer. When measurements were made in air with Teflon AF films that had been soaked in silicone oil, results intermediate between the oil-filled and air-filled conditions were observed, which is consistent with reports that silicone oil impregnation reduces the contact angle hysteresis of Teflon AF films.[27] We also note that at lower voltages in air, slowly moving droplets tended to exhibit somewhat unsteady 'stick-slip' motion, while this was not observed in silicone oil at any speed. Since measurements made in air also tended to be much more dependent on the history and processing conditions of the Teflon AF film we have used mainly silicone oil media in the experimental work reported here.

The scaling properties of droplet transport were investigated with identical scaled arrays of electrode pitch ranging from 150–1500 μm. The ratios DL^{-1} and hL^{-1} were fixed at ~1.3 and ~4.8, respectively, although hL^{-1} was approximately three times as large for the smallest array due to the difficulty of controlling such small gaps in our set-up. The results are plotted in Fig. 7 as average linear velocity, $\bar{v}$, *versus* voltage. Over the range of different system scales, the dependence of $\bar{v}$ on voltage is nearly identical and reaches a value of about 10 cm s^{-1} at approximately 60 V. Beyond 60 V the larger droplets we tested would sometimes split apart during transfer. Smaller volumes are less susceptible to fragmentation and average velocities in excess of 10 cm s^{-1} were obtained for the smaller droplets we tested. Since droplet transfer rates vary inversely with the length scale, transfer rates as high as 1000 Hz were obtained for the smallest electrodes tested. Such rates should permit hundreds of discrete operations to be carried out per second in electrowetting-based systems.

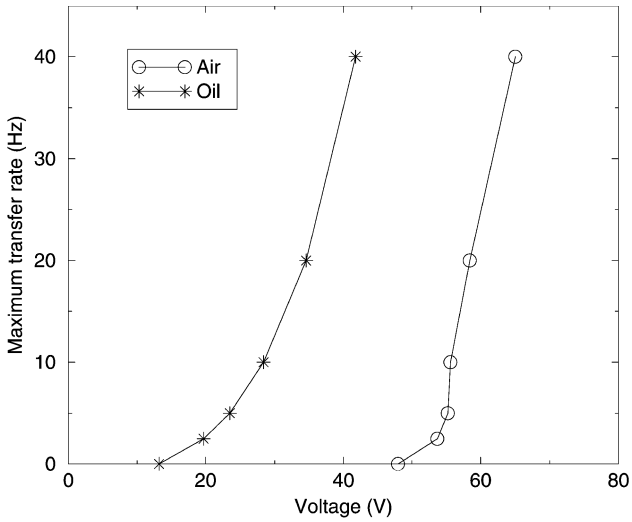

Fig. 6 Effect of medium on droplet transport. The *x*-axis intercept is the minimum voltage at which movement, but incomplete transfer, of the droplet was observed. The droplet was ~900 nl of 0.1 M KCl with $L = 1.5$ mm, and $h = 0.3$ mm.

4 Droplet formation and dispensing

In addition to transport, realization of an electrowetting-based lab-on-a-chip requires certain other microfluidic operations, such as mixing, splitting, and dispensing of microdroplets. Mixing may be accomplished by bringing two droplets into direct contact and allowing them to merge as shown in Fig. 8(D–F). Our observations of droplets doped with dye or fluorescent beads indicate the existence of a recirculating flow inside droplets during transport. Thus, it is expected that simple transport of merged droplets should accelerate mixing and result in mixing times substantially faster than can be achieved through diffusion alone. Once mixed, the combined droplet may be split back into two droplets by energizing the electrodes on either side while grounding the electrode underneath, as shown in Fig. 8(A–C). Through successive merging and splitting operations a variety of mixing and dilution strategies can be implemented.

Formation of unit-sized droplets from a larger initial sample or reagent droplet could be accomplished through a series of binary splitting operations. Alternatively, the unit-sized drop-

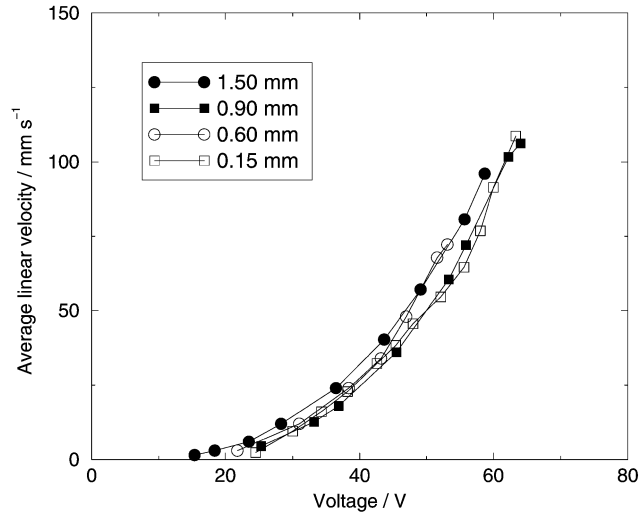

Fig. 7 Effect of scaling on droplet transport. The electrode pitch, gap spacing, and droplet volume were scaled in proportion. The results are plotted as average linear velocity ($\bar{v}$) of the droplet as a function of voltage for transport in 1 cSt silicone oil.

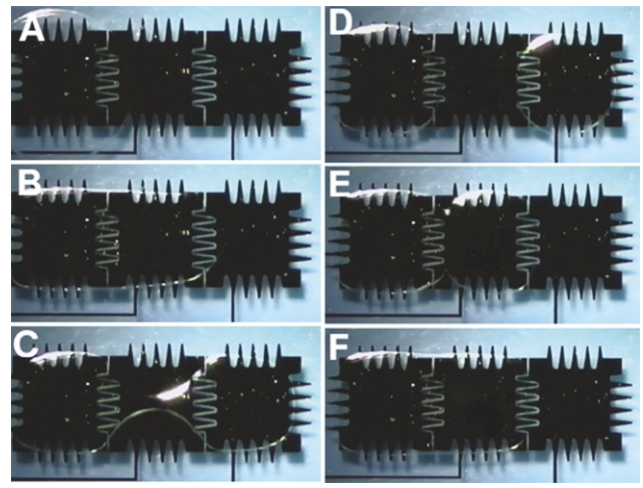

Fig. 8 Time-lapse series, droplet merging and splitting. Initially, only the left electrode is energized (A). The middle electrode is then energized (B) and, after a delay, the voltage is switched from the middle to the right electrode resulting in division of the droplet (C) and (D). The original droplet is then reassembled by switching the voltage on the right electrode back to the middle electrode (E) and (F).

View Article Online

Published on 11 March 2002. Downloaded by Duke University on 10/04/2014 16:28:05.

lets can be asymmetrically dispensed from a larger sample droplet or reagent reservoir as required. In this case, a liquid protrusion or finger connected to the liquid source is first created by energizing a path of electrodes adjacent to the source. After the liquid front has extended across the energized electrodes, one or more of the intermediate electrodes is grounded, causing the finger to break at that location and leaving a newly formed droplet on the terminal energized electrode (Fig. 9). This was the procedure by which the smallest droplets (down to 3 nl) were formed from larger initial droplets in the scaling experiments.

Microdroplets can also be dispensed from a liquid source external to the chip. Consider a droplet of polar liquid surrounded by oil between two hydrophobic surfaces under positive pressure determined by Laplace's Law:

$$\Delta P = \gamma\left(\frac{1}{r_1}+\frac{1}{r_2}\right) \quad (2)$$

where γ is the liquid–liquid interfacial tension and r_1 and r_2 are the principal radii of curvature of the interface. If the liquid communicates with a hole in the top surface of the chip, it tends to withdraw into that hole, provided the hole is large enough. On the other hand, a source of external hydrostatic pressure can be used to drive the liquid back into the chip. Alternating the external pressure, one can drive the liquid inside the chip and let it withdraw. If, during the withdrawal, the receding liquid front encounters a charged control electrode, a droplet conforming to that electrode's dimensions and position is left behind (Fig. 10). This procedure also provides a convenient interface to robotic pipettors for loading and positioning of the initial sample and reagent droplets.

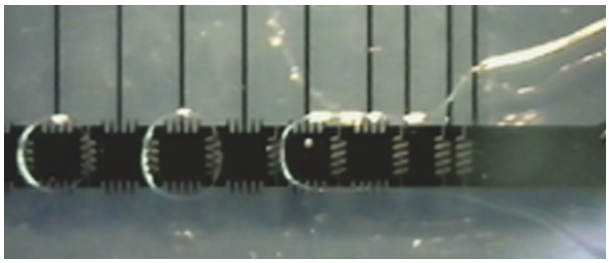

Fig. 9 Dispensing of unit-sized microdroplets from a larger initial droplet located on the chip. A large pad electrode (not visible) fixes the position of the source droplet, while a series of adjacent electrodes are energized to create a finger. The finger is then cut by grounding electrodes between the terminal energized electrode and the liquid source. As the liquid retracts a droplet is left behind. The droplet volumes are about 700 nl.

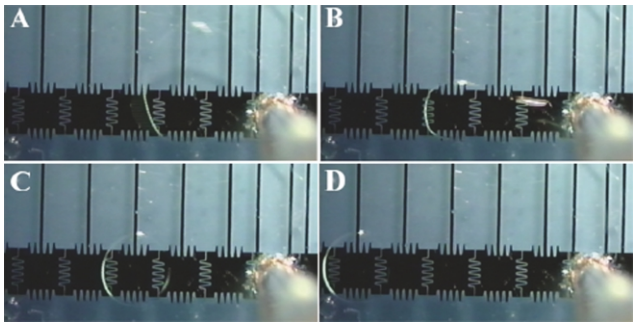

Fig. 10 Time-lapse series, droplet dispensing from an external source. Electrolyte is introduced under pressure through a pipette-tip fitted to a hole in the top-plate (A). The fluid is allowed to retract (B) and a new microdroplet is left on an energized electrode (C). The droplet is then transported away (D) and the process repeated. The total elapsed time is about 2 s and the droplet volume is about 700 nl.

5 Conclusion

Our results demonstrate the feasibility of electrowetting microactuation for manipulation of aqueous droplets ranging from nanoliters to microliters in volume. Dispensing, mixing, splitting and transport of droplets was demonstrated without the use of conventional pumps, valves or channels. Transport of droplets is rapid and repeatable with well over 100000 cycles of transfer having been demonstrated for a single droplet. The maximum average velocity for transport is over 10 cm s^{-1}, which is more than 2000 times faster than reported for light-driven motion[14] and 40 times faster than electrochemical actuation.[12]Although thermocapillary[11]and dielectrophoretic[15] methods can achieve velocities of the same order of magnitude, both methods result in substantial heating of the liquid. With electrowetting high levels of integration and operational flexibility are possible because the operation of the instrument is directly driven by electrical potential, while the use of transparent electrodes also makes electrowetting compatible with optical detection methods.

6 Acknowledgements

The authors thank the Biomedical Microsensors Laboratory at North Carolina State University for their assistance with device microfabrication.

References

1 *Microsystem Technology in Chemistry and Life Sciences*, eds.A. Manz and H. Becker, Springer, Berlin, Germany, 1998.
2 P. Gravesen, J. Branebjerg and O. S. Jensen, *J. Micromech. Microeng.*, 1993, **3**, 168.
3 M. Elwenspoek, T. S. J. Lammerink, R. Mikaye and J. H. J. Fluitman, *J. Micromech. Microeng.*, 1994, **4**, 227.
4 S. Shoji and M. Esashi, *J. Micromech. Microeng.*, 1994, **4**, 157.
5 C. H. Mastrangelo, M. A. Burns and D. T. Burke, *Proc. IEEE*, 1998, **86**, 1769.
6 G. J. M. Bruin, *Electrophoresis*, 2000, **21**, 3931.
7 K. Hosokawa, T. Fujii and I. Endo, *Anal. Chem.*, 1999, **71**, 4781.
8 K. Handique, D. T. Burke, C. H. Mastrangelo and M. A. Burns, *Anal. Chem.*, 2000, **72**, 4100.
9 K. Handique, D. T. Burke, C. H. Mastrangelo and M. A. Burns, *Anal. Chem.*, 2001, **73**, 1831.
10 M. A. Burns, C. H. Mastrangelo, T. S. Sammarco, F. P. Man, J. R. Webster, B. N. Johnson, B. Foerster, D. Jones, Y. Fields, A. R. Kaiser and D. T. Burke, *Proc. Natl. Acad. Sci. U.S.A.*, 1996, **93**, 5556.
11 T. S. Sammarco and M. A. Burns, *AIChE J.*, 1999, **45**, 350.
12 B. S. Gallardo, V. K. Gupta, F. D. Eagerton, L. I. Jong, V. S. Craig, R. R. Shah and N. L. Abbott, *Science (Washington, D.C.)*, 1999, **283**, 57.
13 O. Sandre, L. Gorre-Talini, A. Ajdari, J. Prost and P. Silberzan, *Phys. Rev. E*, 1999, **60**, 2964.
14 K. Ichimura, S. Oh and M. Nakagawa, *Science (Washington, D.C.)*, 2000, **288**, 1624.
15 T. B. Jones, M. Gunji, M. Washizu and M. J. Feldman, *J. Appl. Phys.*, 2001, **89**, 1441.
16 J. Lee and C. J. Kim, *J. Microelectromech. Syst.*, 2000, **9**, 171.
17 M. Washizu, *IEEE Trans. Ind. Appl.*, 1998, **34**, 732.
18 M. G. Pollack, R. B. Fair and A. D. Shenderov, *Appl. Phys. Lett.*, 2000, **77**, 1725.
19 G. Beni and S. Hackwood, *Appl. Phys. Lett.*, 1981, **38**, 207.
20 G. Beni and M. A. Tenan, *J. Appl. Phys.*, 1981, **52**, 6011.
21 E. Colgate and H. Matsumoto, *J. Vac. Sci. Technol., A*, 1990, **8**, 3625.
22 B. Berge, *C.R.A.S. III*, 1993, **317**, 157.
23 J. A. M. Sondag-Huethorst and L. G. J. Fokkink, *Langmuir*, 1994, **10**, 4380.
24 M. Vallet, B. Berge and L. Vovelle, *Polymer*, 1996, **37**, 2465.
25 W. J. J. Welters and L. G. J. Fokkink, *Langmuir*, 1998, **14**, 1535.
26 H. J. J. Verheijen and M. W. J. Prins, *Rev. Sci. Instrum.*, 1999, **70**, 3668.
27 H. J. J. Verheijen and M. W. J. Prins, *Langmuir*, 1999, **15**, 6616.

View Article Online

28 V. Peykov, A. Quinn and J. Ralston, *Colloid Polym. Sci*., 2000, **278**, 789.
29 C. B. Gorman, H. A. Biebuyck and G. M. Whitesides, *Langmuir*, 1995, **11**, 2242.
30 B. Berge and J. Peseux, *Eur. Phys. J. E*., 2000, **3**, 159.
31 M. W. J. Prins, W. J. J. Welters and J. W. Weekamp, *Science (Washington, D.C.)*, 2001, **291**, 277.
32 E. Seyrat and R. A. Hayes, *J. Appl. Phys*., 2001, **90**, 1383.
33 C. Quillet and B. Berge, *Curr. Opin. Colloid Interface Sci*., 2001, **6**, 34.
34 A. Torkkeli, J. Saarilahti, A. Haara, H. Harma, T. Soukka and P. Tolonen, *Proc. IEEE MEMS*, 2000, 475.
35 M. K. Chaudhury and G. M. Whitesides, *Science (Washington, D.C.)*, 1992, **256**, 1539.
36 A. W. Adamson and A. P. Gast, *Physical Chemistry of Surfaces*, Wiley, New York, 1997.

Published on 11 March 2002. Downloaded by Duke University on 10/04/2014 16:28:05.